A Novel Strategy for Numerical Simulation of High-Speed Turbulent Reacting Flows

by

M.R.H. Sheikhi, T.G. Drozda and P. Givi
Department of Mechanical Engineering
University of Pittsburgh
Pittsburgh, PA 15261

Annual Report to
The NASA Langley Research Center

Grant NAG-1-03010

for the Period

January 1, 2003 to December 31, 2003

A Novel Strategy for Numerical Simulation of High-Speed Turbulent Reacting Flows

M.R.H. Sheikhi, T.G. Drozda and P. Givi

Department of Mechanical Engineering

University of Pittsburgh

Pittsburgh, PA 15261

Abstract

The objective of this research is to improve and implement the filtered mass density function (FDF) methodology for large eddy simulation (LES) of high-speed reacting turbulent flows. We have just completed Year 1 of this research. This is the Final Report on our activities during the period: January 1, 2003 to December 31, 2003. 2002.

In the efforts during the past year, LES is conducted of the Sandia Flame D [1,2], which is a turbulent piloted nonpremixed methane jet flame. The subgrid scale (SGS) closure is based on the scalar filtered mass density function (SFMDF) methodology [3]. The SFMDF is basically the mass weighted probability density function (PDF) of the SGS scalar quantities [4]. For this flame (which exhibits little local extinction), a simple flamelet model is used to relate the instantaneous composition to the mixture fraction. The modelled SFMDF transport equation is solved by a hybrid finite-difference/Monte Carlo scheme.

Dr. J. Philip Drummond (Hypersonic Propulsion Branch, NASA LaRC, Mail Stop 197, Tel: 757-864-2298) is the Technical Monitor of this Grant.

1 Introduction

There have been significant recent developments of subgrid scale (SGS) closures for large eddy simulation (LES) of turbulent reacting flows. Several recent reviews are available [4–10]. One such closure is via the filtered density function (FDF) methodology, first introduced by Pope [11]. This is the counterpart of the probability density function (PDF) method which has proven quite effective in Reynolds averaged simulations (RAS) [4,12]. This success is due to the inherent property of the PDF of providing complete statistical information about the variables. Due to this property, the FDF offers the ability to treat finite-rate chemistry and the turbulence-chemistry interactions. In comparison to RAS, the LES/FDF methodology provides a more detailed and reliable prediction of turbulent reacting flows and is better suited to account for the large scale unsteady phenomena which are prevalent in combustion devices. The scalar FDF (SFDF) is considered by many investigators [13–17]. Its extension to account for variable density flows is via the scalar filtered mass density function (SFMDF) [3,18]. The velocity FDF (VFDF) is introduced by Gicquel *et al.*[19] and the velocity-scalar FDF (VSFDF) by Sheikhi *et al.* [20]. A recent review on the state-of-progress on LES/FDF is provided by Givi [10]. The outcome of these investigations has been encouraging, warranting further extension and application of this methodology in turbulent combustion.

In this work, we employ the FDF method for prediction of the piloted jet flame studied in the experiments of the Combustion Research Facility at the Sandia National Laboratories [21,22]. This flame has been the subject of broad investigations by other computational/modelling methodologies [2,23–26]. In the experiments, three turbulent flames are considered: Flames D, E and F.

The geometrical configuration in these flames is the same, but the jet inlet velocity is varied. In Flame D, the fuel jet velocity is the lowest and the flame is close to equilibrium. The jet velocity increases from flames D to E to F, with noticeable non-equilibrium effects in the latter two. Flame D is considered in this work. The objective is to assess the predictive capability of the LES/FDF methodology in capturing the flow field and scalar mixing. This is a necessary step before consideration of the non-equilibrium flames (E and F).

2 Formulation

Sandia Flame D consists of a main jet with a mixture of 25% methane and 75% air by volume. The nozzle is placed in a coflow of air and the flame is stabilized by a substantial pilot. The Reynolds number for the main jet is $Re = 22400$ based on the nozzle diameter $D = 7.2mm$ and the bulk jet velocity $49.6m/sec$. The methane-air reaction mechanism, as occurs in this flame, is taken into account via the "flamelet" model. This model considers a laminar, one-dimensional counterflow (opposed jet) flame configuration [6]. The detailed kinetics mechanism of the Gas Research Institute (GRI2.11) [27] is employed to describe combustion. At low strain rates, the flame is close to equilibrium. Thus, all of the thermo-chemical variables are determined by the "mixture fraction."

Formulation is based on the compressible form of the continuity, Navier-Stokes, energy (enthalpy) and mixture fraction conservation equations in a low Mach number flow [28]. These equations govern the space ($\mathbf{x} \equiv x_i,\ i = 1, 2, 3$) and time ($t$) variations of the fluid density $\rho(\mathbf{x}, t)$, the velocity vector $\boldsymbol{u} \equiv u_i(\mathbf{x}, t)$, the pressure $p(\mathbf{x}, t)$, the specific enthalpy $h(\mathbf{x}, t)$ and the mixture fraction

$\xi(\mathbf{x},t)$. We employ Fourier's law of heat conduction, Fick's law of diffusion and we assume unity Lewis number. The molecular viscosity μ increases with temperature (T) to the power of 0.7. The magnitude of the molecular Schmidt (and Prandtl) number is $Sc = 0.75$.

For LES, we consider a spatially and temporally invariant positive filter $\mathcal{G}(\mathbf{x}'-\mathbf{x})$ of width $\Delta_{\mathcal{G}}$. The filtered value of the variable $Q(\mathbf{x},t)$ is denoted by $\langle Q(\mathbf{x},t)\rangle_\ell$ and its mass-weighted filtered value is denoted by $\langle Q(\mathbf{x},t)\rangle_L = \langle \rho Q\rangle_\ell / \langle\rho\rangle_\ell$. The SFMDF of the mixture fraction is denoted by $\mathcal{F}_L(\psi,\mathbf{x},t)$ where ψ denotes the (probability) composition domain of the mixture fraction. The SFMDF accounts for SGS statistics of only the scalar field. Thus, the closure of the SGS hydrodynamics must be provided by other means. Here, we employ a well-established gradient diffusion model, in which the SGS dynamic viscosity ν_t is modelled by the MKEV (modified kinetic energy viscosity) [3,29] model. In the transport equation governing the SFMDF, the effects of SGS convection are also modelled by an analogous gradient diffusion model. The SGS mixing is closed via the least square mean estimation (LMSE) model [30,31]. These are described in detail in our previous papers on SFDF [3,15]. The final, modelled SFMDF transport equation reads:

$$\frac{\partial \mathcal{F}_L}{\partial t} + \frac{\partial\left[\langle u_i\rangle_L \mathcal{F}_L\right]}{\partial x_i} = \frac{\partial}{\partial x_i}\left[(\gamma+\gamma_t)\frac{\partial\left(\mathcal{F}_L/\langle\rho\rangle_\ell\right)}{\partial x_i}\right] + \frac{\partial}{\partial\psi}\left[\Omega_m\left(\psi-\langle\xi\rangle_L\right)\mathcal{F}_L\right]. \tag{1}$$

Here, $\gamma = \frac{\mu}{Sc}$ is the molecular diffusivity, $\gamma_t = \frac{\langle\rho\rangle_\ell \nu_t}{Sc_t}$ is the SGS diffusivity and $Sc_t = 0.75$ is the SGS Schmidt number. With the closure as such, the modelled scalar flux is consistent with that in most other (non-FDF) methods

[32,33]:

$$\langle\rho\rangle_\ell \left[\langle u_i\xi\rangle_L - \langle u_i\rangle_L \langle\xi\rangle_L\right] = -\gamma_t \frac{\partial \langle\xi\rangle_L}{\partial x_i}. \tag{2}$$

The term Ω_m is the SGS mixing frequency (as required in LMSE) and is modelled by [15,3] $\Omega_m = C_\Omega(\gamma + \gamma_t)/(\langle\rho\rangle_\ell \Delta_G^2)$, with $C_\Omega = 8$.

The relation between the thermo-chemical variables (denoted by the array $\boldsymbol{\phi}(\mathbf{x}, t)$) and the mixture fraction is provided by the flamelet library. In the context of the opposed jet flame, the library provides: $\boldsymbol{\phi} = \boldsymbol{\phi}(\xi, a)$ where a denotes the strain rate. For a fixed value of a, the SGS statistics of the thermo-chemical variables are determined from the SFMDF:

$$\langle\boldsymbol{\phi}(\mathbf{x}, t)\rangle_L = \frac{1}{\langle\rho\rangle_\ell} \int \boldsymbol{\phi}(\xi) \mathcal{F}_L(\xi, \mathbf{x}, t) d\xi. \tag{3}$$

A hybrid finite-difference (FD) / Monte Carlo (MC) scheme is employed to solve the coupled set of the SFMDF equation and the filtered hydrodynamics equations. In this scheme, the domain is discretized by FD grid points and the SFMDF is represented via an ensemble of MC particles [34]. All of the hydrodynamic variables are determined on the FD points. A fourth order compact scheme [35,36] is used for FD discretization. Transport of the MC particles and the change in their properties are described by a set of stochastic differential equations (SDEs) similar to those describing a diffusion process [37]. The MC particles undergo motion in physical space by convection due to the filtered flow velocity and diffusion due to molecular and SGS diffusivities. The compositional value of each particle is changed due to SGS mixing. These are described by the SDEs:

$$dx_i^+ = \left[\langle u_i\rangle_L + \frac{1}{\langle\rho\rangle_\ell} \frac{\partial(\gamma + \gamma_t)}{\partial x_i}\right] dt + \sqrt{2(\gamma + \gamma_t)/\langle\rho\rangle_\ell}\ dw_i, \tag{4}$$

$$d\xi^+ = -\Omega_m \left[\xi^+ - \langle\xi\rangle_L\right] dt, \tag{5}$$

where x_i^+ and ξ^+ denote Lagrangian position and the composition (mixture fraction), respectively. The term w denotes the Wiener process [38]. The Fokker-Planck equation corresponding to Eqs. (4)-(5) is equivalent to Eq. (1). Thus, the solution of these SDEs represent the FMDF in the probabilistic sense.

To understand the operational procedure, the elements of the computation are shown in Fig. 1. For simplicity, a two-dimensional domain is shown with fixed grid spacing of size of Δ. The MC particles are distributed randomly and are free to move within the domain as governed by Eq. (4). This transport is Lagrangian, thus the solution is free of the constraints associated with typical simulation of convection on fixed grid points. Statistical information, *e.g.* filtered values, at any point is obtained by considering an ensemble of N_E computational particles residing within an ensemble domain of side length Δ_E centered around the points. For reliable statistics with minimal numerical dispersion, it is desired to minimize the size of ensemble domain and maximize the number of the MC particles [12]. In this way, the ensemble statistics would tend to the desired filtered values

$$\langle Q \rangle_E \equiv \frac{1}{N_E} \sum_{n \in \Delta_E} Q^{(n)} \xrightarrow[\substack{N_E \to \infty \\ \Delta_E \to 0}]{} \langle Q \rangle_L \tag{6}$$

where $Q^{(n)}$ denotes the information carried by n^{th} MC particle pertaining to transport variable Q. Transfer of information from the grid points to the MC particles is accomplished via interpolation. The transfer of information from the particles to the grid points is accomplished via ensemble averaging.

In the hybrid scheme, some of the filtered quantities are obtained by MC, some by FD and some by *both*. That is, there is a "redundancy" in determination of some of the quantities. This redundancy is very useful in monitoring the

consistency of the simulated results [39]. In general, all of the equations for the filtered quantities can be solved by FD, where all of the unclosed terms are evaluated by MC. This process can be done at any filtered moment level [19]. Here, the filtered values of the mixture fraction and the temperature are used to establish consistency. Some results in this regard are presented in the next section. In addition, the computational accuracy of the methodology is established by examining both the statistical and the dispersion errors [40]. In doing so, the correlation of the fluid density with distribution of the MC particles, the size of the ensemble domain, the number of particles within this domain and the global distribution of the particles are monitored in a manner similar to that reported in our previous work [3,15,19,20].

3 Results

In the simulations, all of the flow variables at the inflow are set the same as those in the experiments, including the inlet profiles of the velocity and the mixture fraction. The flow is excited by superimposing oscillating axisymmetric and helical perturbations at the inflow. The procedure is similar to that of Danaila and Boersma [41], but is modified to match the experimental data in the near field. Simulations are conducted on a three-dimensional Cartesian mesh with uniform spacings in each of the three directions. The computational domain spans a region of $18D \times 10D \times 10D$ in streamwise, and the two lateral directions. The number of grid points are $91 \times 101 \times 101$, respectively. The filter size is set equal to $\Delta_G = 2(\Delta x \Delta y \Delta z)^{(1/3)}$ where Δx, Δy and Δz denote the grid spacings in streamwise (x) and the two lateral ($y - z$) directions, respectively. The size of the ensemble domain for evaluations of the filtered

values from the MC solver is equal to the filter size. There are approximately 48 MC particles at each grid point for these evaluations. In total, there are about 3.4 million MC particles within the domain at all times.

The flamelet table at strain rate of $a = 100\ 1/s$ is used to relate the thermochemical variables to the mixture fraction. First, the consistency and accuracy of the computations are assessed. Next, the overall predictive capability of LES/SFMDF is demonstrated by comparing the flow statistics with the Sandia data. These statistics are obtained by long-time averaging of the filtered field. The notations $\overline{Q}$ and $RMS(Q)$ denote, respectively, the time-averaged mean and root mean square values of the variable Q.

The simplest consistency check is via flow visualization. For example, Fig. 2 shows the instantaneous contours of the filtered temperature field as obtained by the FD and the MC methods. The central jet lies in the middle along the axial coordinate, surrounded by a pilot where the temperature is the highest and encircled by the air coflow. The region close to inlet is dominated by the molecular diffusion and the jet exhibits a laminar-like behavior. Farther downstream, the growth of perturbations is manifested by the formation of large scale coherent vortices. The upstream feedback from the vortices created initially is sufficient to trigger self-sustaining vortex rollup and subsequent pairing and coalescence of neighboring vortices. Due to presence of helical instabilities, the layer is asymmetric. The similarity of the results in the two figures is observed at all other times and is also observed for the mixture fraction (not shown). This consistency is further assessed via establishing identical statistics of the redundant quantities as generated by the two methods.

The capability of the method in predicting the hydrodynamics field is demon-

strated by examining some of the (reported) flow statistics. The centerline mean and RMS values of the axial velocity are compared to experimental data in Fig. 3. This figure indicates that the flow is adequately excited and the predicted results are in good agreement with data. The statistics of the thermo-chemical variables are also compared with corresponding data. The measurements are exhaustive; here, only some sample results are shown. The radial ($r = \sqrt{z^2 + y^2}$) distribution of the mixture fraction is shown to compare well with data (Fig. 4a). Similar agreement is observed at other streamwise locations. The mean temperature values in Fig. 4b indicate a slight over-prediction on the rich side. This is due to premixing of methane with air as also indicated previously [25]. The "resolved" RMS values of the mixture fraction and temperature are in good agreement with data. However, the "total" RMS values, including the contributions of both the resolved and the SGS fields, are higher than values reported experimentally. The contribution of the SGS to the total scalar energy is about 30% which is expected in LES. The higher values of the total RMS values as predicted by LES/FD are not due to MC numerical dispersion because the FD results do indeed yield the same values. The level of SGS variance can be decreased by increasing the magnitude of C_Ω. However, this would not alter the total RMS values significantly. It is possible that some contribution of this variance is not included in the measurements due to finite probe size. Higher resolution measurements would determine the allocations of scalar variance to the resolved and SGS fields.

The statistics of the mass fractions (denoted by Y) of several of the species are compared with data in Fig. 5. Similar to the temperature results on the rich side, the reactants' mass fractions are under-predicted slightly, while the products are over-predicted. The mean values of the mass fractions of the major

and the minor species compare well with experimental data. All of the results indicate the adequacy of the flamelet table in relating the thermo-chemical variables to the mixture fraction, and also the good predictive capability of the SFMDF for this flame. The level of agreement of the RMS values of the mass fraction is the same as that presented in Fig. 4.

The computational costs associated with LES/FDF depends, obviously, on the parameters of the simulations. For the case reported here, the simulations required about 110 hours of CPU time on a SUN Fire 4800 with 6 processors. This includes the times required for consistency tests and ensemble averaging of data. The computational time for LES without including SGS effects is about 10-12 times less. However such simulations yield erroneous predictions and in many cases lead to numerical instabilities. For further comparative assessment of the computational requirements of the FDF in comparison to non-FDF methods, we refer to our previous work[3,15,19,20].

4 Summary and Concluding Remarks

The filtered density function (FDF) methodology [11] is now at a stage that it can be used for prediction of complex turbulent reacting flows. This is demonstrated in this work by utilizing the simplest form of the FDF for large eddy simulation (LES) of a piloted, nonpremixed, turbulent, methane jet flame (Sandia Flame D). For this near-equilibrium flame, the thermo-chemical variables are related to the mixture fraction. This is done by construction of a flamelet library (in a counter-flow jet flame) in which the chemical reaction is modelled by detailed kinetics [27]. It is useful to note that the approach here is fundamentally different from those followed in previous flamelet based

SGS models. In most previous contributions [25,42–45], the FDF of the mixture fraction is *assumed* (*e.g.* beta or other distribution). Here, a modelled transport equation for the mass weighted FDF of the mixture fraction [3] is considered. This equation is solved by a hybrid finite-difference / Monte Carlo method. After establishing the consistency and accuracy of the hybrid solver, the predictive capability of the overall scheme is assessed by comparison with experimental data. For these comparisons, the ensemble (long time averaged) values of the thermo-chemical variables are considered. It is shown that all of the mean quantities are, generally, predicted well. The resolved RMS of the variables also compare well with data. However, when the contribution of the subgrid scale (SGS) quantities are included, the experimental data are over-predicted.

There are two ways by which this work can be continued. First, is extension of LES/SFMDF for prediction of flames which experience extinction (such as Sandia Flames E and F) and/or re-ignition. This would provide a more definitive assessment of the predictive capabilities of the FDF. Such simulations require consideration of finite-rate chemistry, as demonstrated in RAS/PDF simulations of Sandia flames [23,24]. Presently, it is not computationally feasible to implement detailed kinetics in such simulations. But implementation of reduced kinetics schemes using in situ adaptive tabulation, such as those used in RAS/PDF [23,24] is within reach. Second, it is desirable to implement the LES/VSFDF [20] for prediction of this (or other complex) flame(s). In VSFDF, the SGS convection appears in a closed form, thus the assumption of gradient diffusion can be relaxed. This is also feasible within the near future. Accomplishments of both of these tasks can be expedited by further reduction of the computational requirements of the FDF. The present work establishes

the capability of LES/FDF for accurate prediction of complex flames, warranting its further use for modelling of even more complex turbulent reacting flows.

References

[1] R. S. Barlow, J. I. Frank, Effects of turbulence on species mass fractions in methane/air jet flames, Proc. Combust. Inst. 27 (1998) 1087–1095.

[2] R. S. Barlow, Sandia National Laboratories, TNF Workshop website, `http://www.ca.sandia.gov/tdf/Workshop.html` (2003).

[3] F. A. Jaberi, P. J. Colucci, S. James, P. Givi, S. B. Pope, Filtered mass density function for large eddy simulation of turbulent reacting flows, J. Fluid Mech. 401 (1999) 85–121.

[4] S. B. Pope, Turbulent Flows, Cambridge University Press, Cambridge, UK, 2000.

[5] R. W. Bilger, Future progress in turbulent combustion research, Prog. Energy Combust. Sci. 26 (4-6) (2000) 367–380.

[6] N. Peters, Turbulent Combustion, Cambridge University Press, Cambridge, UK, 2000.

[7] E. S. Oran, J. P. Boris, Numerical Simulation of Reactive Flows, 2nd Edition, Cambridge University Press, New York, NY, 2001.

[8] T. Poinsot, D. Veynante, Theoretical and Numerical Combustion, R. T. Edwards, Inc., Philadelphia, PA, 2001.

[9] D. Veynante, L. Vervisch, Turbulent combustion modeling, Prog. Energ. Combust. 28 (3) (2002) 193–301.

[10] P. Givi, Subgrid scale modeling in turbulent combustion: A review, AIAA Paper 2003-5081 (2003).

[11] S. B. Pope, Computations of turbulent combustion: Progress and challenges, Proc. Combust. Inst. 23 (1990) 591–612.

[12] S. B. Pope, PDF methods for turbulent reactive flows, Prog. Energy Combust. Sci. 11 (1985) 119–192.

[13] F. Gao, E. E. O'Brien, A large-eddy simulation scheme for turbulent reacting flows, Phys. Fluids A 5 (6) (1993) 1282–1284.

[14] J. Réveillon, L. Vervisch, Subgrid-scale turbulent micromixing: Dynamic approach, AIAA J. 36 (3) (1998) 336–341.

[15] P. J. Colucci, F. A. Jaberi, P. Givi, S. B. Pope, Filtered density function for large eddy simulation of turbulent reacting flows, Phys. Fluids 10 (2) (1998) 499–515.

[16] X. Y. Zhou, J. C. F. Pereira, Large eddy simulation (2D) of a reacting plan mixing layer using filtered density function, Flow, Turbulence and Combustion 64 (2000) 279–300.

[17] C. M. Cha, P. Troullet, A subgrid-scale mixing model for large-eddy simulations of turbulent reacting flows using the filtered density function, Phys. Fluids 15 (6) (2003) 1496–1504.

[18] S. James, F. A. Jaberi, Large scale simulations of two-dimensional nonpremixed methane jet flames, Combust. Flame 123 (2000) 465–487.

[19] L. Y. M. Gicquel, P. Givi, F. A. Jaberi, S. B. Pope, Velocity filtered density function for large eddy simulation of turbulent flows, Phys. Fluids 14 (3) (2002) 1196–1213.

[20] M. R. H. Sheikhi, T. G. Drozda, P. Givi, S. B. Pope, Velocity-scalar filtered density function for large eddy simulation of turbulent flows, Phys. Fluids 15 (8) (2003) 2321–2337.

[21] P. A. Nooren, M. Versiuis, T. H. Van der Meer, R. S. Barlow, J. H. Frank, Raman-Rayleigh-LIF measurements of temperature and species concentrations in the Delft piloted turbulent jet diffusion flame, Applied Physics B71 (2000) 95–111.

[22] Sandia National Laboratories, Combustion Research Facility website, `http://www.ca.sandia.gov/tdf/` (2002).

[23] Q. Tang, J. Xu, S. B. Pope, Pdf calculations of local extinction and NO production in piloted-jet turbulent methane/air flames, Proc. Combust. Inst. 28 (2000) 133–139.

[24] J. Xu, S. B. Pope, Pdf calculations of turbulent nonpremixed flames with local extinction, Combust. Flame 123 (2000) 281–307.

[25] H. Pitsch, H. Steiner, Large eddy simulation of a turbulent piloted methane/air diffusion flame (Sandia flame D), Phys. Fluids 12 (10) (2000) 2541–2554.

[26] H. Steiner, W. K. Bushe, Large eddy simulation of a turbulent reacting jet with conditional source-term estimation, Phys. Fluids 13 (3) (2001) 754–759.

[27] G. P. Smith, D. M. Golden, M. Frenklach, N. W. Moriarty, B. Eiteneer, M. Goldenberg, C. T. Bowman, R. Hanson, S. Song, W. C. Gardiner, V. Lissianski, Z. Qin, `http://www.me.berkeley.edu/gri_mech`

[28] F. A. Williams, Combustion Theory, 2nd Edition, The Benjamin/Cummings Publishing Company, Menlo Park, CA, 1985.

[29] J. Bardina, J. H. Ferziger, W. C. Reynolds, Improved turbulence models based on large eddy simulations of homogeneous, incompressible, turbulent flows,

Department of Mechanical Engineering Report TF-19, Stanford University, Stanford, CA (1983).

[30] E. E. O'Brien, The probability density function (PDF) approach to reacting turbulent flows, in: P. A. Libby, F. A. Williams (Eds.), Turbulent Reacting Flows, Springer-Verlag, Heidelberg, 1980, Ch. 5, pp. 185–218.

[31] R. Borghi, Turbulent combustion modeling, Prog. Energy Combust. Sci. 14 (1988) 245–292.

[32] T. M. Eidson, Numerical simulation of the turbulent rayleigh-benard problem using subgrid modelling, J. Fluid Mech. 158 (1985) 245–268.

[33] P. Moin, W. Squires, W. H. Cabot, S. Lee, A dynamic subgrid-scale model for compressible turbulence and scalar transport, Phys. Fluids A 3 (1991) 2746–2757.

[34] S. B. Pope, Particle method for turbulent flows: Integration of stochastic model equations, J. Comp. Phys. 117 (1995) 332–349.

[35] J. P. Drummond, M. H. Carpenter, D. W. Riggins, Mixing and mixing enhancement in supersonic reacting flow fields, in: S. N. B. Murthy, E. T. Curran (Eds.), High Speed Propulsion Systems, Vol. 137 of AIAA Progress Series, American Institute of Aeronautics and Astronautics, 1991, Ch. 7, pp. 383–455.

[36] C. A. Kennedy, M. H. Carpenter, Several new numerical methods for compressible shear-layer simulations, Appl. Num. Math. 14 (1994) 397–433.

[37] C. W. Gardiner, Handbook of Stochastic Methods, Springer-Verlag, New York, NY, 1990.

[38] S. Karlin, H. M. Taylor, A Second Course in Stochastic Processes, Academic Press, New York, NY, 1981.

[39] M. Muradoglu, S. B. Pope, D. A. Caughey, The hybrid method for the PDF equations of turbulent reactive flows: Consistency conditions and correction algorithms, J. Comp. Phys. 172 (2001) 841–878.

[40] J. Xu, S. B. Pope, Assessment of numerical accuracy of PDF/Monte Carlo methods for turbulent reacting flows, J. Comp. Phys. 152 (1999) 192–230.

[41] I. Danaila, B. J. Boersma, Direct numerical simulation of bifurcating jets, Phys. Fluids 12 (5) (2000) 1255–1257.

[42] S. M. De Bruyn Kops, J. J. Riley, G. Kosály, A. W. Cook, Investigation of modeling for non-premixed turbulent combustion, Combust. Flame 60 (1998) 105–122.

[43] P. E. DesJardin, S. H. Frankel, Two-dimensional large eddy simulation of soot formation in the near-field of a strongly radiating nonpremixed acetylene-air turbulent jet flame, Combust. Flame 119 (1999) 121–132.

[44] A. Kempf, H. Forkel, J. Y. Chen, A. Sadiki, J. Janicka, Large-eddy simulation of a counterflow configuration with and without combustion, Proc. Combust. Inst. 28 (2000) 35–40.

[45] F. Ladeinde, X. Cai, B. Sekar, B. Kiel, Application of combined LES and flamelet modeling to methane, propane, and jet-A combustion, AIAA Paper 2001-0634 (2001).

List of Figures

All Figures

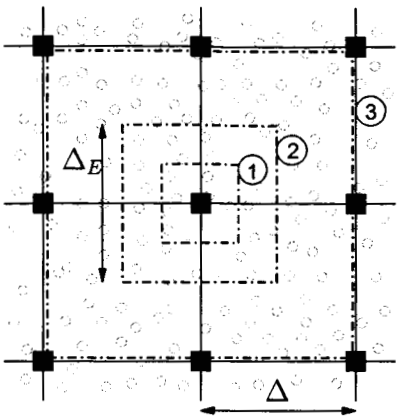

Fig. 1. Elements of computation as used in a typical LES/FDF. Solid squares denote the FD points and the circles denote the MC particles. Also shown are three different ensemble domains.

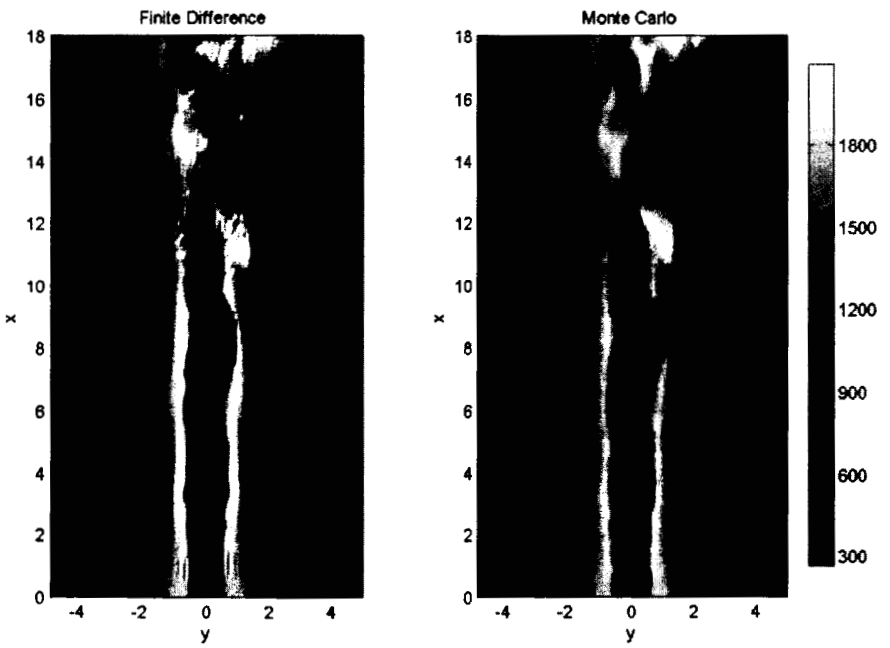

Fig. 2. Instantaneous contours of the filtered values of the temperature (K) as obtained by FD and MC simulations.

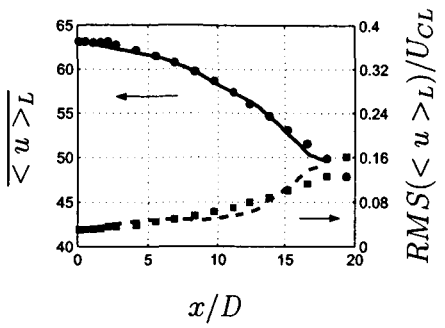

Fig. 3. The mean and RMS values of the axial velocity $[m/s]$ at the centerline. U_{CL} denotes the mean axial velocity at the centerline, the symbols denote experimental data and the lines denote the predictions.

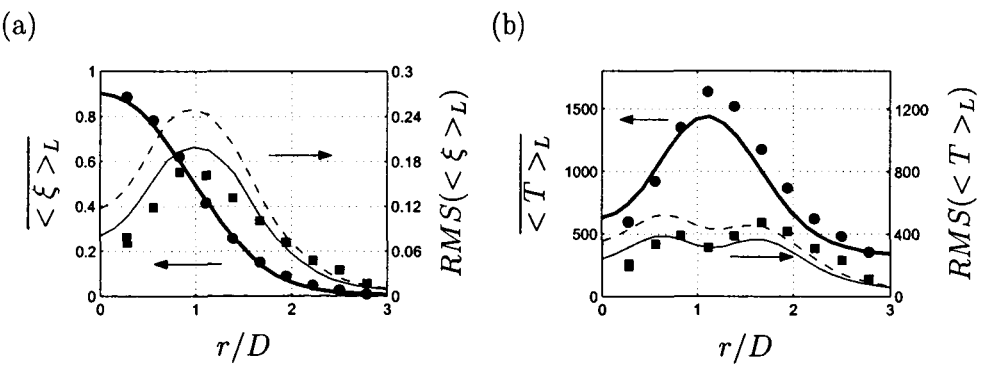

Fig. 4. Radial distributions of the mean and RMS values at $x/D = 15$. The symbols denote experimental data. The thick lines denote the mean values, the thin solid lines denote the resolved RMS values and the thin dashed lines denote total RMS values. (a) Mixture fraction, (b) temperature.

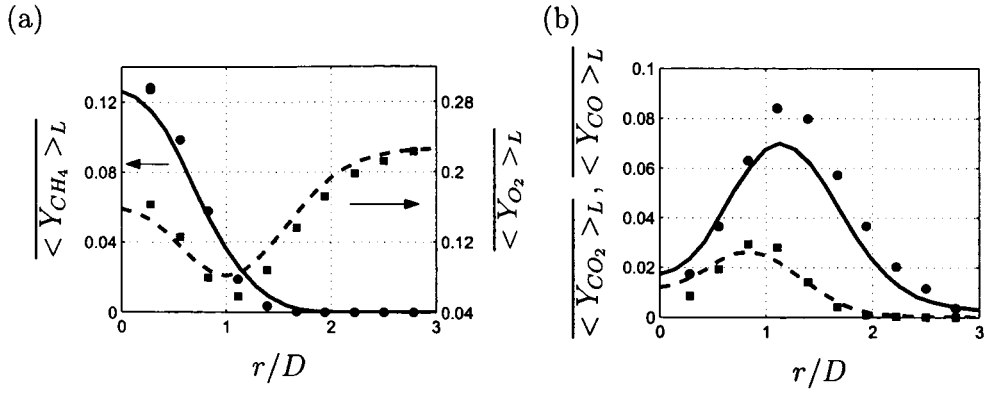

Fig. 5. Radial distribution of the mean values of the mass fractions at $x/D = 15$. The symbols denote experimental data. (a) Solid line: CH_4; dashed line: O_2, (b) solid line: CO_2; dashed line: CO.